

Adding Multimodal Controls to Whole-body Human Motion Generation

Yuxuan Bian¹, Ailing Zeng^{2*}, Xuan Ju¹, Xian Liu¹, Zhaoyang Zhang¹, Wei Liu², Qiang Xu^{1*}

¹The Chinese University of Hong Kong ²Tencent
<https://yxbian23.github.io/ControlMM>

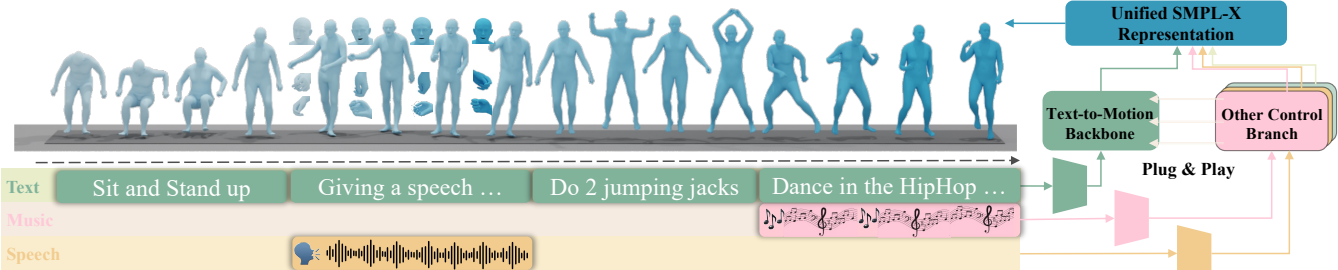


Figure 1: We present *ControlMM*, a whole-body motion generation framework with plug-and-play multimodal control, which can generalize robust motion generation abilities across Text-to-Motion, Speech-to-Gesture, and Music-to-Dance.

Abstract

Whole-body multimodal motion generation, controlled by text, speech, or music, has numerous applications including video generation and character animation. However, employing a unified model to accomplish various generation tasks with different condition modalities presents two main challenges: motion distribution drifts across different generation scenarios and the complex optimization of mixed conditions with varying granularity. Furthermore, inconsistent motion formats in existing datasets further hinder effective multimodal motion generation. In this paper, we propose *ControlMM*, a unified framework to **Control** whole-body **M**ultimodal **M**otion generation in a plug-and-play manner. To effectively learn and transfer motion knowledge across different motion distributions, we propose *ControlMM-Attn*, for parallel modeling of static and dynamic human topology graphs. To handle conditions with varying granularity, *ControlMM* employs a coarse-to-fine training strategy, including stage-1 text-to-motion pre-training for semantic generation and stage-2 multimodal control adaptation for conditions of varying low-level granularity. To address existing benchmarks' varying motion format limitations, we introduce *ControlMM-Bench*, the first publicly available multimodal whole-body human motion generation benchmark based on the unified whole-body SMPL-X format. Extensive experiments show that *ControlMM* achieves state-of-the-art performance across various standard motion generation tasks.

Introduction

Whole-body human motion generation with multimodal control (Zhang et al. 2024b; Liu et al. 2024a; Li et al. 2023), which produces natural and logical human movements based on multimodal conditions, has many downstream applications, including human video generation (Hu 2024) and character animation (Zhang et al. 2023a).

* Corresponding authors.

Recent advancements in single-conditioned human motion generation have enabled realistic human motion generation under control signals from varying modalities, including text descriptions (Guo et al. 2022; Zhang et al. 2023c), music clips (Siyao et al. 2022; Li et al. 2023), and speech segments (Liu et al. 2024a; Chen et al. 2024). However, achieving whole-body motion generation with multimodal control in a unified model encounters several serious challenges: **① Motion distribution drift:** The motion distribution in generated tasks corresponding to different control signals exhibits significant distribution drift. Under limited available motion data compared with video/text, current methods struggle to transfer robust motion topology knowledge across different multimodal motion generation scenarios (Ling et al. 2023; Zhang et al. 2024b). **② Struggling optimization under mixed conditions:** Current multimodal motion generation methods mainly choose to compress control signals of varying granularity into a shared latent space to learn the multimodal conditioned generation abilities (Zhou, Wan, and Wang 2023; Zhang et al. 2024b), leading to alignment issues across different modalities and optimization confusion when learning conditions at different granularity simultaneously. **③ Non-uniform motion format and evaluation:** There are no multimodal whole-body human motion generation benchmarks with unified motion format and evaluation pipelines, impeding this field's progress.

► **Motion distribution drift:** Under different control signals, the motion distribution often varies significantly (Zhang et al. 2024b; Ling et al. 2023). In text-to-motion (T2M), semantic text guidance mainly controls daily torso movements (Guo et al. 2022; Lin et al. 2023), while speech in speech-to-gesture (S2G) emphasizes influence on gestures and facial expressions (Liu et al. 2024a; Yi et al. 2023). Music-to-dance (M2D) includes a more dynamic and variable correlation between the third-perspective mu-

sic with limb and hand movements (Li et al. 2023). Previous research has typically focused on a single task to avoid the weak generative transferability posed by distribution drifts. However, inspired by human kinematics (Loper et al. 2015; Pavlakos et al. 2019), we analyzed the distributions of T2M, S2G, and M2D and found that motion distributions can be decomposed into static human topology structures and complementary dynamic topology relationships. Therefore, we propose parallel modeling of static and dynamic human topology graphs to obtain transferable topology knowledge across different tasks.

- **Struggling optimization under mixed conditions:** Current multimodal motion generation work often compresses different control signals (semantic text guidance, low-level speeches on first-person perspective and the low-level music on third-person perspective) into a latent space for mixed modeling, including transformer token embedding (Zhou, Wan, and Wang 2023) and ImageBind’s (Girdhar et al. 2023) hidden space (Zhang et al. 2024b). However, due to the significant information gaps between different modalities, such compression and mixed learning leads to notable optimization burden (Team et al. 2023). Therefore, we choose to introduce different control signals through separate control branches and conduct a coarse-to-fine progressive training strategy to cultivate generation abilities under conditions of varying granularity. This also provides our model with plug-and-play, user-friendly, and efficient training properties.
- **Non-uniform motion format and evaluation:** Finally, there are no high-quality multimodal whole-body human motion generation benchmarks with unified motion representation and evaluation pipelines, which prompted us to build the first such benchmarks based on the SMPL-X (Pavlakos et al. 2019) whole-body format.

In this work, we aim to develop a unified framework to **Control** whole-body **Multi-modal Motion** generation in a plug-and-play manner, **ControlMM**, that can address motion distribution drifts in different generation scenarios and progressively learn different conditions of varying granularity. Based on human motion kinematics and distribution analysis using t-distributed stochastic neighbor embedding, we find that motion distributions corresponding to different control signals can be decomposed into static human topology structures and complementary dynamic topology relationships, which can be generalized across different generation scenarios. Thus, we design **ControlMM-Attn** to model such human-centric spatiotemporal properties, where the spatial branch learns and transfers motion knowledge across different motion distributions by parallel modeling of static and dynamic human topology graphs, and the temporal branch learns the universal motion sequence relationships. Based on **ControlMM-Attn**, **ControlMM** employs a two-stage coarse-to-fine generation framework. In the first stage, it learns coarse semantic motion generation abilities under coarse-grained text guidance. In the second stage, control branches are added to the stage-1 frozen backbone to inherit semantic generation capabilities and achieve fine-grained plug-and-play control for specified conditions with-

out optimization confusion brought by mixed training.

To address existing benchmarks’ varying motion format limitations, we also built **ControlMM-Bench**, the first publicly available multimodal human motion generation benchmark based on the unified whole-body representation SMPL-X, including unified data construction and evaluation pipelines. Extensive experiments show that **ControlMM** achieves competitive performance across various standard motion generation tasks, including text-to-motion, speech-to-gesture, and music-to-dance, compared to state-of-the-art baselines. We also provide extensive ablation studies offering valuable insights into model design, training strategies, and scaling effects for future multimodal whole-body human motion generation foundation models.

Briefly put, our contributions can be summarized as:

- In this work, we decompose the motion distribution drift modeling in multimodal generation into the static human skeleton structure capture and dynamic topology relationship measurement. For the first time, our **ControlMM-Attn** achieves parallel modeling of such human-centric spatial properties to boost whole-body motion generation against distribution drifts under varying conditions.
- We introduce **ControlMM**, a two-stage coarse-to-fine multimodal motion generation framework that decouples the conditioned generation learning process of control signals at different granularities, enabling efficient and plug-and-play multimodal motion generation training.
- We develop **ControlMM-Bench**, the first publicly available multimodal whole-body motion generation benchmark with unified representation. Extensive experiments show that **ControlMM** achieves competitive performance across various standard motion generation tasks.

Related Works

Human Motion Generation Models

Conditioned human motion generation models have extensive downstream applications, including text-to-motion (T2M), speech-to-gesture (S2G), and music-to-dance (M2D). In text-to-motion, models (Tevet et al. 2023; Chen et al. 2023; Zhang et al. 2023b; Liu et al. 2023; Zhang et al. 2024a, 2023c; Liang et al. 2024) achieve text-controlled motion generation with semantic consistency by applying advanced generative models and aligning motion and text feature domains. For speech-to-gesture (Yi et al. 2023; Chen et al. 2024; Liu et al. 2022b), many efforts focus on mapping speech to human gestures through rhythm alignment and character style learning. Additionally, numerous studies (Li et al. 2023; Tseng, Castellon, and Liu 2023; Siyao et al. 2022) design spatial and temporal coherence constraints to ensure that models learn the corresponding style and rhythm from the input music. Recently, increasing attention has been given to multimodal human motion generation (Zhou, Wan, and Wang 2023; Ling et al. 2023; Zhang et al. 2024b; Luo et al. 2024). M^3 -GPT (Luo et al. 2024) injects quantized compressed tokens of different modalities into the extended vocabulary of a large language model, achieving motion understanding and generation while ignoring the modeling of human topology prior.

Table 1: **Comparison of *ControlMM* with Previous Motion Generation Methods.** *ControlMM* jointly models the static human skeleton structure and dynamic human topology relationships to achieve flexible motion knowledge transfer across various whole-body generation scenarios, supporting plug-and-play with any new control signal modality.

| Model | Text2Motion | Music2Dance | Speech2Gesture | Static Body Prior | Dynamic Body Adaption | Whole Body | Unified Representation | Plug-and-Play |
|-----------------------------------|-------------|-------------|----------------|-------------------|-----------------------|------------|------------------------|---------------|
| FineMoGen (Zhang et al. 2023c) | ✓ | ✗ | ✗ | ✓ | ✗ | ✗ | ✗ | ✗ |
| HumanTomato (Lu et al. 2023) | ✓ | ✗ | ✗ | ✓ | ✗ | ✓ | ✗ | ✗ |
| FineDance (Li et al. 2023) | ✗ | ✓ | ✗ | ✗ | ✗ | ✗ | ✗ | ✗ |
| Bailando (Siyao et al. 2022) | ✗ | ✓ | ✗ | ✓ | ✗ | ✗ | ✗ | ✗ |
| EMAGE (Liu et al. 2024a) | ✗ | ✗ | ✓ | ✓ | ✗ | ✓ | ✗ | ✗ |
| TalkShow (Yi et al. 2023) | ✗ | ✗ | ✓ | ✓ | ✗ | ✓ | ✗ | ✗ |
| MCM (Ling et al. 2023) | ✓ | ✓ | ✓ | ✗ | ✗ | ✗ | ✗ | ✓ |
| Motion-Verse (Zhang et al. 2024b) | ✓ | ✓ | ✓ | ✓ | ✓ | ✓ | ✗ | ✗ |
| <i>ControlMM</i> | ✓ | ✓ | ✓ | ✓ | ✓ | ✓ | ✓ | ✓ |

Motion-Verse (Zhang et al. 2024b) introduces dynamic attention scores to measure the relationships between different body parts, but it overlooks modeling the general basic static human topology, resulting in limited generalization and increased optimization difficulty. Additionally, it adopts the mixed training strategies for all conditions based on ImageBind (Girdhar et al. 2023), causing model confusion when learning conditions of varying granularity simultaneously and significant computation costs when re-training for new control signals. MCM (Ling et al. 2023) attempts to address the optimization confusion brought by mixed training based on utilizing the ControlNet (Zhang, Rao, and Agrawala 2023) architecture, but its channel-based attention design fails to capture either the static or the dynamic skeletal topology, resulting in poor generalization across generation scenarios. Moreover, MCM also only focuses on tensor movements, lacking the ability to generate whole-body motion. Compared with previous methods in Tab. 1, *ControlMM* achieve whole-body motion generation under varying control signals with plug-and-play control by adopting *ControlMM-Attn* to parallel capture the static human topology structure and domain-specific dynamic skeleton relationships, and conducting the coarse-to-fine conditioned generation training strategy.

Human Motion Generation Benchmarks

Various conditioned human motion generation datasets have been constructed in recent years. For text-to-motion, researchers have curated datasets encompassing action categories (Carreira et al. 2019; Chung et al. 2021; Gu et al. 2018; Liu et al. 2019; Trivedi, Thatipelli, and Sarvadevabhatla 2021), sequential action labels (Taheri et al. 2020; Zhang et al. 2022; Guo et al. 2020; Ionescu et al. 2013; Punakkal et al. 2021), and arbitrary natural language descriptions (Lin et al. 2023; Guo et al. 2022; Tang et al. 2023) at various abstraction levels. Specifically, AMASS (Mahmood et al. 2019) consolidates 15 optical marker-based motion capture datasets into a comprehensive collection based on SMPL (Loper et al. 2015) representation. HumanML3D (Guo et al. 2022) extracted a high-quality subset within AMASS based on H3D format for torso-only generation, including three arbitrary natural language descriptions per motion clip from diverse annotators. For music-to-dance (Li et al. 2022; Zhuang et al. 2022), the most popular dataset is AIST++ (Li et al. 2021), which reconstructs 5 hours of dance based on SMPL format from videos, despite its significant reconstruction error, and lacks capture of hand movements. Finedance (Li et al. 2023) addresses these limi-

tations by collecting 14.6 hours across 22 dance genres and supplementing the dataset with detailed hand modeling using the SMPL-H (Pavlakos et al. 2019) based representation. For speech-to-gesture, datasets (Liu et al. 2024a, 2022a; Yi et al. 2023; Ginosar et al. 2019) are gathered from pseudo-labeled (PGT) and motion-captured sources. Mocap datasets are generally preferred due to significant errors in monocular 3D pose estimation in PGT (Gärtner et al. 2022). Recently, BEATS2 (Liu et al. 2024a) and BEATS (Liu et al. 2022a) have emerged as the most popular benchmarks, celebrated for their diverse range of motion and extensive data volume. BEATS2, building upon BEATS, utilizes SMPL-X (Pavlakos et al. 2019) and FLAME (Kim, Kim, and Choi 2023) to achieve higher-quality unified mesh-level data. Despite these developments, there is no publicly available benchmark that supports unified representation for multimodal whole-body motion generation.

Motivation

The key challenge in achieving whole-body human motion generation with multimodal control is addressing motion distribution drift across different generation scenarios (Zhang et al. 2024b) and the efficient learning of control signals at varying granularities (Ling et al. 2023).

Motion distribution drift solution. Current human motion generation models mainly focus on scenarios guided by a single control condition since they struggle to handle the noticeable motion distribution drift across different scenarios (Zhou, Wan, and Wang 2023). For instance, as shown in Fig. 3, text-to-motion primarily involves everyday torso movements, speech-to-gesture includes complex hand gestures, rich facial expressions, and almost stationary lower limbs, while music-to-dance emphasizes varied and extensive limb movements with limited hand movements. However, many human-centric studies (Zeng et al. 2021) have confirmed that representing the human skeletal topology as a directed weighted graph, with different parts as vertices, can introduce human kinematic priors in complex motion scenarios, thereby improving model generalization under distribution shifts. Additionally, based on human kinematic (Loper et al. 2015; Pavlakos et al. 2019), it is natural to decompose human topology into a combination of dynamic and static skeleton graphs in various scenarios. For instance, in any scenario, the root vertex (hip) always significantly influences its child vertices (lower limbs), with symmetrical interactions between pairs of arms. However, in speech-to-gesture scenarios, the linkage between the lower limbs and other body parts weakens significantly, while the

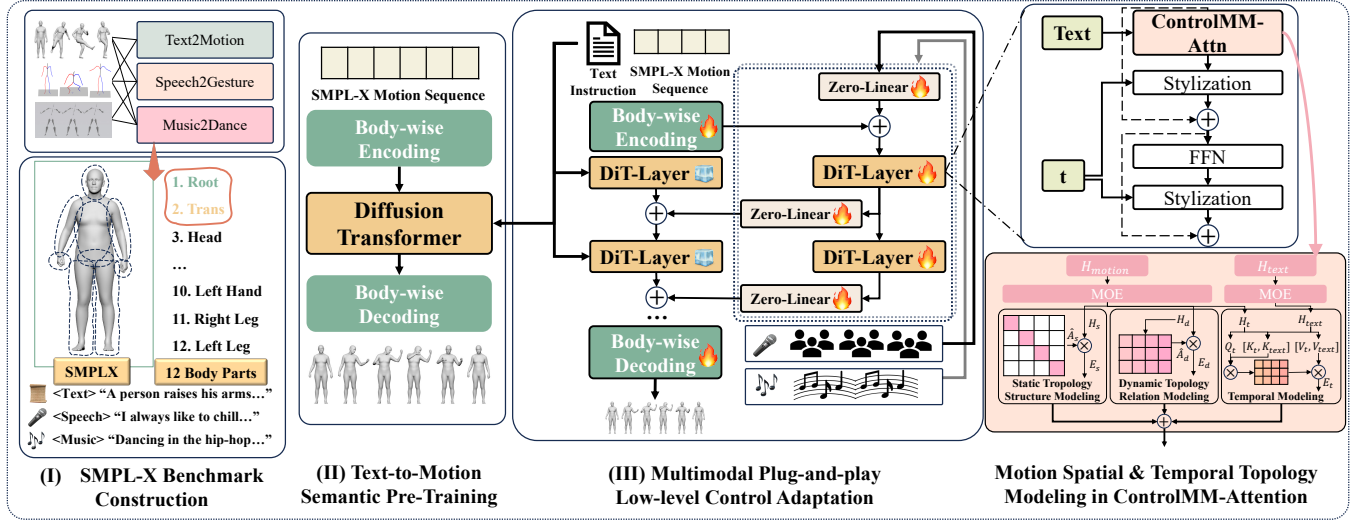


Figure 2: **Architecture of ControlMM.** *ControlMM* is a transformer-based diffusion model. In the first stage, *ControlMM* uses texts as a semantic control guide to learn coarse-grained cross-scenario motion knowledge across multiple datasets; in the second stage, *ControlMM* freezes the backbone while adding a plug-and-play control branch to learn the different low-level control signals. The core of *ControlMM* is *ControlMM-Attn*, which optimizes the representation of motion token sequences by capturing the spatial properties of dynamic and static human topology graphs and learning temporal relationships in parallel.

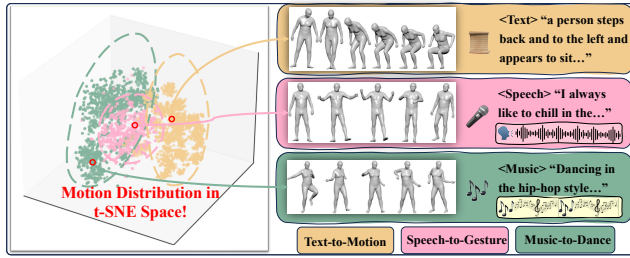


Figure 3: **The t-SNE latent space.** It clearly illustrates the motion distribution drift across different generation tasks. However, all scenarios share the basic static human skeleton structure, with only the dynamic skeleton relationships varying according to the specific generation scenario.

edge weight between hands and facial expressions strengthens. Therefore, modeling both dynamic and static topological graphs can efficiently generalize human motion knowledge across different tasks, even with limited data and significant distribution drifts.

Efficient learning of conditions at varying granularities. Different motion generation scenarios correspond to different control conditions at varying granularities. For instance, text guidance typically provides sequence-level coarse-grained semantic control, while first-perspective speech and third-perspective music focus more on frame-level low-level control (Liu et al. 2024a; Li et al. 2023). Mixed learning of all control signals within a single compressed latent space leads to inevitable modality alignment loss and fails to decouple the learning process for each granularity (Zhang, Rao, and Agrawala 2023; Ling et al. 2023), causing optimization confusion. Motivated by other vision generation paradigms in the image/video domain, including StableDiffusion (Rombach et al. 2022) and Sora (Liu et al. 2024b), decoupling the conditioned generation under different con-

trol signals and using T2X as a fundamental pretraining task can establish robust generative capabilities for subsequent multi-condition generation, resulting in more efficient and fine-grained multimodal control generation capabilities.

Method

ControlMM Framework

The overview of *ControlMM* is described in Fig. 2. Aimed at decoupling the conditioned generation learning at varying granularities, we adopt a two-branch architecture consisting of a main text-to-motion branch and a plug-and-play low-level control branch, along with a two-stage coarse-to-fine training strategy to efficiently grasp the motion topology knowledge across different scenarios with various control signal modalities. The main branch is a motion diffusion transformer specially designed with *ControlMM-Attn* for static and dynamic motion topology characteristics. The control branch shares the same structure as the main branch and is initialized with the well-trained parameters of the main branch, trained through extensive semantic-aligned text-to-motion training.

Stage ① Text-to-Motion Semantic Pre-training. The main branch $f_m(\cdot)$ is optimized in Stage I, text-to-motion semantic pre-training, using text-to-motion paired data collected from diverse scenarios in *ControlMM-Bench*. We choose text as the shared condition among various unimodal datasets, allowing *ControlMM* to acquire sequence-level generation and coarse-grained text-guidance following abilities between text $\mathbf{H}_{text} \in \mathbb{R}^{B \times F_t \times D_t}$ and motion $\mathbf{H}_{motion} \in \mathbb{R}^{B \times F_m \times D_m}$. Furthermore, text guidance pre-training in diverse generation scenarios helps follow fine-grained control of other low-level conditions in Stage II.

Stage ② Multimodal Low-level Control Adaptation. During the low-level control adaptation fine-tuning stage,

we aim to model the correlation between various condition signals $\mathbf{H}_c \in \mathbb{R}^{B \times T_c \times D_c}$ and motion sequences $\mathbf{H}_{motion} \in \mathbb{R}^{B \times F_m \times D_m}$. All main branch parameters $f_m(\cdot)$ are frozen to maintain their coarse-grained motion generation and semantic text guidance following abilities. A copy of the main branch parameters $\hat{f}_m(\cdot)$ is then used to initialize the control branch, connecting them with a zero-initialized linear layer $\mathbf{W}_p \in \mathbb{R}^{D_m \times D_m}$ to prevent early training noise from causing collapse (Zhang, Rao, and Agrawala 2023). Then the condition signals (speech, music, or other low-level control signals) are fed into the control branch, where a position mask $\mathbf{M}_c \in \{0, 1\}^{F_m}$ aligns the condition signals to the motion sequence length F_m , setting zeros for the $F_m - T_c$ missing frames in the original control signal sequence. Next, we employ position embeddings $\mathbf{H}_p \in \mathbb{R}^{F_m \times D_m}$ to explicitly align each frame of the motion sequence with the condition signals. Also, we randomly mask the condition signals with a probability of 10% to achieve classifier-free guidance. The output of each control branch layer is directly added to the corresponding main branch layer input through the zero bridge linear, allowing new control signals to guide frame-level human motion generation.

ControlMM-Attn Architecture

The core of *ControlMM* is *ControlMM-Attn*, which parallel captures the static and dynamic human topology graphs, thereby enhancing the transferability of motion topology knowledge across diverse generation scenarios against non-neglectable distribution drift. *ControlMM-Attn* has three key components: a static-skeleton graph learner and a dynamic-topology relationship graph learner for parallel modeling spatial properties of human motion, and temporal attention for modeling the frame-level dynamics of each body part over time. The three modules share the same motion representation input $\mathbf{H}_m \in \mathbb{R}^{B \times F_m \times D_m}$, which is the output of the last *ControlMM-Attn* layer refined further by a MOE(Shazeer et al. 2017) layer.

For the static-skeleton graph learner, it first constructs the N_b graph vertex representation $\mathbf{H}_s \in \mathbb{R}^{B \times F_m \times N_b \times D_b}$, and then initializes a diagonal unit matrix $\mathbf{A}_s \in \mathbb{R}^{N_b \times N_b}$ as the adjacency matrix of the initial body static structure topology graph \mathcal{G}_s , where each body part is only connected to itself (to prevent training collapse caused by random connections). Through optimization in diverse motion generation tasks, this adjacency matrix $\hat{\mathbf{A}}_s$ captures static, input-independent human topology structure, allowing the model to quickly establish a fundamental understanding of human topology for new control-based generation scenarios even with limited data. The output of this module is $\mathbf{E}_s = \hat{\mathbf{A}}_s \cdot \mathbf{H}_s$.

While capturing static human topology graphs can grasp basic human topology structure and help the model converge quickly in a new distribution, they are independent of the input and fail to adapt dynamically to new generation contexts (Zhang et al. 2024b). This can lead to underfitting in scenarios requiring the generation under new conditions. Therefore, we introduced a dynamic-topology relationship graph learner to aid in modeling the dynamic distribution features, allowing modeling of the distribution

drift corresponding to different control signals when combined with learned static topological structure. This has been proven effective in various human-centric tasks (Zeng et al. 2021). Specifically, the dynamic-topology relationship graph learner treats each body part as a dynamic graph vertex $\mathbf{H}_d \in \mathbb{R}^{B \times F_m \times N_b \times D_b}$, using attention scores $\mathbf{A}_d \in \mathbb{R}^{B \times F_m \times N_b \times N_b}$ as edge weights in the human topology dynamic graph \mathcal{G}_d , further enhancing the model's adaptive spatial structure relationship modeling capability apart from the static-skeleton learner. Its final output is $\mathbf{E}_d = \mathbf{A}_d \cdot \mathbf{H}_d$.

Various studies have shown that basic attention is sufficient for modeling temporal relationships (Nie et al. 2022; Bian et al. 2024). Therefore, we chose to use each body part as a unit $\mathbf{H}_t \in \mathbb{R}^{B \cdot N_b \times F_m \times D_b}$ and measure the temporal relationships between frames based on attention (Vaswani et al. 2017). Considering that external textual control signals are mostly sequential instructions in the temporal dimension, text information is also modeled here to produce the output, $\hat{\mathbf{E}}_t = \text{Softmax}(\mathbf{Q}_{H_t} \cdot [\mathbf{K}_{H_t}^T, \mathbf{K}_{H_{text}}^T] / \sqrt{D_b}) \cdot [\mathbf{V}_{H_t}^T, \mathbf{V}_{H_{text}}^T]$, where $\mathbf{Q}_{H_t} = \mathbf{W}^{Q_{H_t}} \mathbf{H}_t$, $\mathbf{K}_{H_t} = \mathbf{W}^{K_{H_t}} \mathbf{H}_t$, $\mathbf{K}_{H_{text}} = \mathbf{W}^{K_{H_{text}}} \mathbf{H}_{text}$, $\mathbf{V}_{H_t} = \mathbf{W}^{V_{H_t}} \mathbf{H}_t$, $\mathbf{V}_{H_{text}} = \mathbf{W}^{V_{H_{text}}} \mathbf{H}_{text}$, and $[,]$ denotes concat operation. Other sequential control modalities, such as speech and music, are modeled in the control branch. The final output $\mathbf{E} = \mathbf{E}_s + \mathbf{E}_d + \mathbf{E}_t$ of *ControlMM-Attn* combines the spatiotemporal representations of the human skeleton and the temporal structure of each body part.

ControlMM-Bench Construction

To avoid information loss from aligning different motion representations, we selected HumanML3D (Guo et al. 2022) in SMPL format for Text-to-Motion, FineDance (Li et al. 2023) in SMPL-H Rot-6D format for Music-to-Dance, and BEATS2 (Liu et al. 2024a) in SMPL-X format for Speech-to-Gesture from public datasets, which are the most representative unimodal datasets in their respective fields. To support whole-body multimodal control human motion generation, we first processed all data into SMPL-X format. Key operations include filling in missing facial information in HumanML3D and FineDance with average expressions, converting the original FineDance data from SMPL-H Rot-6D format to axis-angle representation for direct alignment with SMPL-X parameters, which is more efficient than the official body-retargeting method with almost no alignment errors. We then pre-trained a motion encoder and a text encoder by aligning text and motion contrastively with a retrieval optimization goal (Lu et al. 2023) for our unified evaluation of the SMPL-X motion representation. For FineDance and BEATS2, which lack corresponding textual information, we generated pseudo-captions to serve as textual inputs, such as "A dancer is performing a Jazz dance in the street style to the rhythm of the wildfire" and "A person is giving a speech, and the content is ...".

Experiments

Implementation Details

We designed two model variants for the first stage of Text-to-Motion backbone training, *ControlMM-Basic* and *Con-*

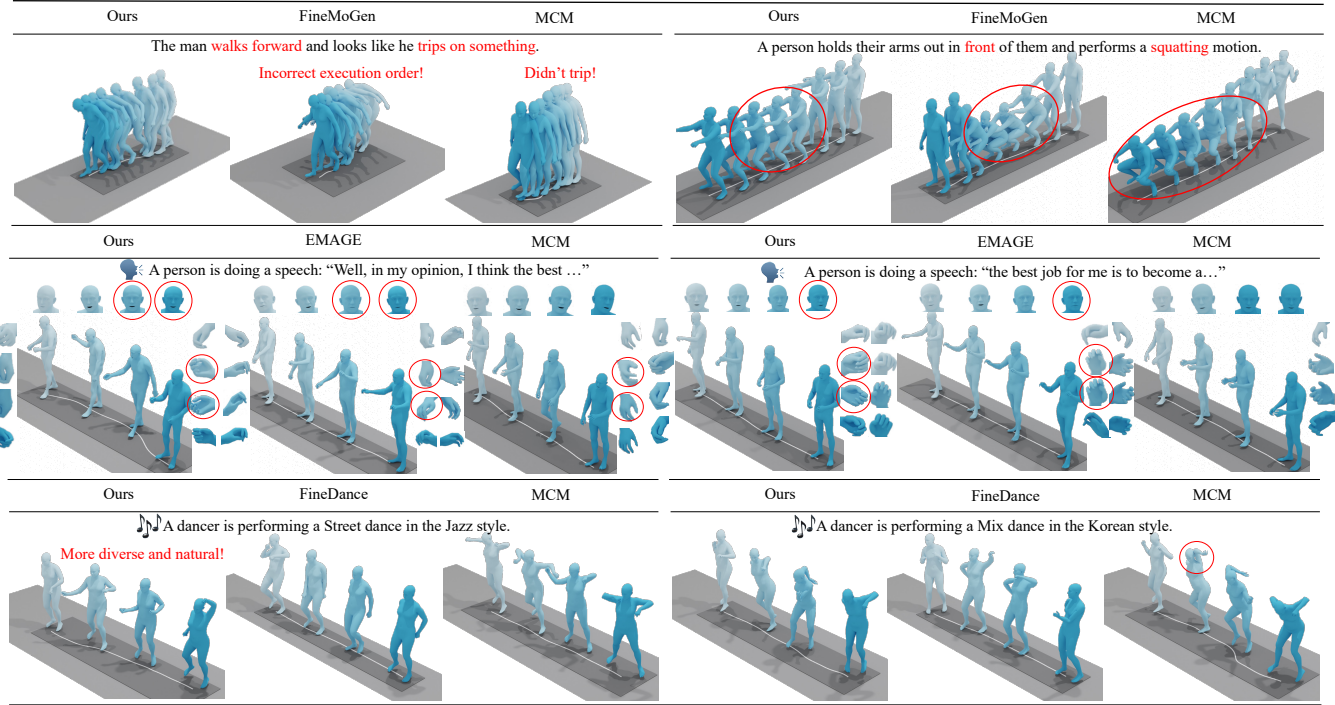


Figure 4: The qualitative results of *ControlMM* and other state-of-the-art baselines in three representative tasks, text-to-motion, speech-to-gesture, and music-to-dance. More visualization is on our website and supplementary.

trolMM-Mix, which were trained on the HumanML3D subset in *ControlMM-Bench* and the entire *ControlMM-Bench*, respectively. In the second stage, we used BEATS2 (Liu et al. 2024a), a large dataset for speech gesture synthesis, and FineDance (Li et al. 2023), a high-quality and extensive choreography dataset, to train control branches for Speech-to-Gesture and Music-to-Dance. *ControlMM*-Basic and *ControlMM*-Mix share the same 4-layer transformer backbone configuration, dividing the body topology into 12 parts, each with a body-part hidden encoding dimension of 64. In both stages, we used the same optimizer, initially iterating for 10 epochs with a learning rate of 2×10^{-4} , followed by 14 epochs with a learning rate of 2×10^{-5} . As described in Sec. , *ControlMM-Bench* used a unified whole-body motion format SMPL-X (Pavlakos et al. 2019), so we retrained the motion encoder and text encoder based on the SMPL-X format using OpenTMR (Lu et al. 2023) for evaluation across any generation scenarios, without being limited by the specific requirements of sub-tasks.

Evaluation Metrics

Text-to-Motion. We use Fréchet Inception Distance (**FID**) to measure the distribution distance between generated motion and the motion ground truth, and diversity (**Div**) to measure the average pairwise Euclidean distance among random pairs of all generated motion sequences. Furthermore, we use **R-Precision** to measure how often the top-k closest motions in Euclidean distance to their corresponding captions are achieved within a 32-sample batch. Finally, we employ Multi-Modal Distance (**MM Dist**) to quantify the average Euclidean distance between motion feature representations and their corresponding text description features.

Speech-to-Gesture. We use FID_H , FID_B , and Div for quality and diversity measurement. FID_H represents the difference between the hand motion distribution and the ground truth hand motion distribution, while FID_B focuses on the distance between the distributions of whole-body motion. Moreover, we found that the speaker’s facial expressions and the synchronization between overall motion and speech rhythm are crucial for the quality of the generated motion. Therefore, we use the Beat Alignment Score (Li et al. 2021) to measure the alignment between the motion and speech beats and employ Face L2 Loss to calculate the difference between generated and real facial expressions.

Music-to-Dance. Similar to Speech-to-Gesture, we use FID_H , FID_B , and Div to measure the quality of music-to-motion generation for hand and whole-body movements, as well as the diversity of the generated motions.

Quantitative and Qualitative Results

We evaluate *ControlMM* on three representative tasks: ① Text-to-Motion, ② Speech-to-Gesture, and ③ Music-to-Dance, analysing both quantitative and qualitative results. When calculating metrics, missing facial information is filled with zero values for both generated motion and ground truth to avoid affecting the evaluation results. More visualization is on our website and supplementary.

Comparison on Text-to-Motion. In the text-to-motion task, we compare *ControlMM* with current SOTA baselines (Zhang et al. 2023c; Ling et al. 2023; Zhang et al. 2024b,a; Tevet et al. 2023; Zhang et al. 2023b) in two benchmarks: the original HumanML3D (Guo et al. 2022) with the tensor-only format and the HumanML3D subset with

| Method | R Precision | | | FID \downarrow | Div \uparrow | MM Dist \downarrow |
|-----------------------------------|-------------------|-------------------|-------------------|-------------------|-------------------|----------------------|
| | Top-1 \uparrow | Top-2 \uparrow | Top-3 \uparrow | | | |
| GT | 0.511 \pm 0.003 | 0.703 \pm 0.003 | 0.797 \pm 0.002 | 0.002 \pm 0.000 | 9.503 \pm 0.065 | 2.974 \pm 0.008 |
| T2M-GPT(Zhang et al. 2023b) | 0.491 \pm 0.003 | 0.680 \pm 0.003 | 0.775 \pm 0.002 | 0.116 \pm 0.004 | 9.761 \pm 0.081 | 3.118 \pm 0.011 |
| MDM(Tevet et al. 2023) | 0.418 \pm 0.005 | 0.604 \pm 0.005 | 0.707 \pm 0.004 | 0.489 \pm 0.025 | 9.450 \pm 0.066 | 3.630 \pm 0.023 |
| MotionDiffuse(Zhang et al. 2024a) | 0.491 \pm 0.001 | 0.681 \pm 0.001 | 0.782 \pm 0.001 | 0.630 \pm 0.001 | 9.410 \pm 0.049 | 3.113 \pm 0.001 |
| FineMoGen(Zhang et al. 2023c) | 0.504 \pm 0.002 | 0.690 \pm 0.002 | 0.784 \pm 0.002 | 0.151 \pm 0.008 | 9.263 \pm 0.094 | 2.998 \pm 0.008 |
| Motion-Verse(Zhang et al. 2024b) | 0.496 \pm 0.002 | 0.685 \pm 0.002 | 0.785 \pm 0.002 | 0.415 \pm 0.002 | 9.176 \pm 0.074 | 3.087 \pm 0.012 |
| MCM(Ling et al. 2023) | 0.494 \pm 0.003 | 0.682 \pm 0.005 | 0.777 \pm 0.003 | 0.075 \pm 0.003 | 9.484 \pm 0.074 | 3.086 \pm 0.011 |
| <i>ControlMM</i> -Basic | 0.501 \pm 0.003 | 0.697 \pm 0.003 | 0.796 \pm 0.002 | 0.173 \pm 0.002 | 9.543 \pm 0.098 | 3.025 \pm 0.008 |

Table 2: **Results of text-to-motion in origin HumanML3D benchmark.** We compare the results of text-to-motion generation between ours and the SOTA methods. Our method achieves better semantic relevance, fidelity, and diversity performances. Indicate best results , indicates second best results .

| Method | R Precision | | | FID \downarrow | Div \uparrow | MM Dist \downarrow |
|-----------------------------------|-------------------|-------------------|-------------------|--------------------|--------------------|----------------------|
| | Top-1 \uparrow | Top-2 \uparrow | Top-3 \uparrow | | | |
| GT | 0.663 \pm 0.006 | 0.807 \pm 0.002 | 0.864 \pm 0.002 | 0.000 \pm 0.000 | 36.423 \pm 0.183 | 15.567 \pm 0.036 |
| T2M-GPT(Zhang et al. 2023b) | 0.529 \pm 0.004 | 0.652 \pm 0.003 | 0.732 \pm 0.003 | 10.457 \pm 0.108 | 36.114 \pm 0.098 | 17.029 \pm 0.039 |
| MDM(Tevet et al. 2023) | 0.376 \pm 0.005 | 0.524 \pm 0.002 | 0.604 \pm 0.001 | 20.849 \pm 0.340 | 36.030 \pm 0.052 | 18.805 \pm 0.014 |
| MotionDiffuse(Zhang et al. 2024a) | 0.527 \pm 0.010 | 0.670 \pm 0.008 | 0.741 \pm 0.008 | 11.740 \pm 0.303 | 35.841 \pm 0.229 | 17.188 \pm 0.043 |
| FineMoGen(Zhang et al. 2023c) | 0.557 \pm 0.011 | 0.712 \pm 0.007 | 0.782 \pm 0.009 | 8.317 \pm 0.165 | 36.538 \pm 0.102 | 16.504 \pm 0.054 |
| MCM(Ling et al. 2023) | 0.416 \pm 0.006 | 0.563 \pm 0.003 | 0.643 \pm 0.001 | 15.906 \pm 0.103 | 35.554 \pm 0.053 | 18.525 \pm 0.055 |
| <i>ControlMM</i> -Basic | 0.590 \pm 0.003 | 0.743 \pm 0.002 | 0.804 \pm 0.004 | 8.477 \pm 0.102 | 36.210 \pm 0.089 | 16.252 \pm 0.035 |
| <i>ControlMM</i> -Mix | 0.597 \pm 0.006 | 0.744 \pm 0.005 | 0.806 \pm 0.003 | 8.001 \pm 0.165 | 36.149 \pm 0.114 | 16.247 \pm 0.047 |

Table 3: **Results of text-to-motion in HumanML3D of *ControlMM-Bench*.** We compare the results of text-to-motion between ours and the SOTA methods. *ControlMM* achieves better semantic relevance, fidelity, and diversity performances. Compared with the original HumanML3D benchmark, the performance differences between different models are more obvious, while maintaining the consistent ranking order, and the GT performance metrics no longer fall below the baselines. This demonstrates that *ControlMM-Bench* provides a more comprehensive performance evaluation based on the unified whole-body representation. Indicate best results , indicates second best results .

| Method | $FID_H \downarrow$ | $FID_B \downarrow$ | Face L2 Loss \downarrow | Beat Align Score \uparrow | Div \uparrow |
|-------------------------|--------------------|--------------------|---------------------------|-----------------------------|----------------|
| Talkshow | 26.713 | 74.824 | 7.791 | 6.947 | 13.472 |
| EMAGE | 39.094 | 90.762 | 7.680 | 7.727 | 13.065 |
| MCM | 23.946 | 71.241 | 16.983 | 7.993 | 13.167 |
| <i>ControlMM</i> -Basic | 18.486 | 27.023 | 10.097 | 8.098 | 10.334 |
| <i>ControlMM</i> -Mix | 12.882 | 25.187 | 8.906 | 8.226 | 12.595 |

Table 4: **Results of speech-to-gesture in BEATS2 of *ControlMM-Bench*.** We evaluate the FID_H and FID_B , Face L2 Loss $\times 10^{-8}$, Beat Align Score $\times 10^{-1}$, and diversity between our and SOTA methods. Indicate best results , indicates second best results .

whole-body representation SMPL-X in *ControlMM-Bench*. The detailed results are shown in Tab. 2 and Tab. 3. In both benchmarks, *ControlMM* achieved better text-guided generation capability, diversity, and motion generation quality. Notably, in the HumanML3D subset with SMPL-X format in *ControlMM-Bench*, the inadequate evaluation abilities in the original HumanML3D benchmark with torso-only representation were significantly improved, providing a more comprehensive and objective comparison. This is because the whole-body SMPL-X representation requires the model to generate the torso movements, gestures, and expressions comprehensively rather than only focusing on the body.

Additionally, we found that *ControlMM*-Mix trained on the *ControlMM-Bench* in the first stage has a significant advantage over *ControlMM*-Basic. This is because *ControlMM*-Mix can efficiently transfer human topology knowledge against distribution drift by parallel modeling static and

dynamic topology in mixed-generation tasks. Qualitative results are as shown in Fig. 4, and *ControlMM* can follow diverse textual descriptions with fine-grained control.

Comparison on Speech-to-Gesture. In Tab. 4, we compared *ControlMM* with MCM (Ling et al. 2023), Talkshow (Yi et al. 2023), and EMAGE (Liu et al. 2024a). Our model achieved good quality and diversity in both hand and whole-body motion generation and excelled in aligning with the rhythm of first-perspective speech. This is credited to our coarse-to-fine training strategy and the robust topology knowledge learned from the static and dynamic human topology graphs. However, in facial motion, *ControlMM*-Mix performs slightly worse than EMAGE and Talkshow. This arises from origin data construction limitations in HumanML3D and FineDance, where the face was filled with random or average expressions, confusing the first training stage that affects speech-to-gesture generation in the second stage. Still, we find *ControlMM*-Mix possesses a notable performance boost against *ControlMM*-Basic, further confirming that *ControlMM*-Attn learned robust topology knowledge that can be generalized across different generation scenarios. Qualitative results in Fig. 4 clearly show that *ControlMM* can effectively follow the speech rhythms and generate reasonable gestures and lip movements.

Comparison on Music-to-Dance. Our model, *ControlMM*, achieves performance comparable to the current

| Method | | HumanML3D (Text-to-Motion) | | | | | BEATS2 (Speech-to-Gesture) | | | | | Finedance (Music-to-Dance) | | |
|---|--------------------------------------|----------------------------|------------------|------------------|------------------|----------------|-------------------------------|-------------------------------|-----------------------------|----------------|-------------------------------|-------------------------------|----------------|--|
| Dynamic-Spatial | Static-Spatial | Top-1 \uparrow | Top-2 \uparrow | Top-3 \uparrow | FID \downarrow | Div \uparrow | FID _H \downarrow | FID _B \downarrow | Beat Align Score \uparrow | Div \uparrow | FID _H \downarrow | FID _B \downarrow | Div \uparrow | |
| ✗ | ✗ | 0.583 | 0.729 | 0.794 | 8.911 | 35.954 | 15.587 | 31.839 | 7.908 | 11.752 | 7.088 | 150.733 | 17.984 | |
| ✗ | ✓ | 0.557 | 0.706 | 0.772 | 9.041 | 36.101 | 12.929 | 27.928 | 8.077 | 12.230 | 5.104 | 112.186 | 18.503 | |
| ✓ | ✗ | 0.582 | 0.732 | 0.798 | 8.455 | 36.241 | 15.517 | 28.631 | 7.708 | 11.313 | 4.972 | 102.103 | 16.385 | |
| ✓ | ✓ | 0.597 | 0.744 | 0.806 | 8.001 | 36.149 | 12.882 | 25.187 | 8.226 | 12.595 | 4.825 | 124.935 | 20.742 | |
| w/ Body En(De)c* Freeze. | | - | - | - | - | - | 19.768 | 28.426 | 8.055 | 10.389 | 3.858 | 76.248 | 16.667 | |
| w/o Body En(De)c* Freeze. | | - | - | - | - | - | 18.486 | 27.023 | 8.098 | 10.334 | 4.067 | 94.965 | 16.365 | |
| <i>ControlMM</i> -Tiny-(4, 64, 77M) | | 0.597 | 0.744 | 0.806 | 8.001 | 36.149 | 12.882 | 25.187 | 8.226 | 12.595 | 4.825 | 124.935 | 20.742 | |
| <i>ControlMM</i> -Small-(4, 128, 130M) | | 0.603 | 0.749 | 0.809 | 7.245 | 36.106 | 12.397 | 24.471 | 8.209 | 12.713 | 4.792 | 119.232 | 21.095 | |
| <i>ControlMM</i> -Small-(8, 64, 145M) | | 0.608 | 0.751 | 0.811 | 7.025 | 36.174 | 13.702 | 22.095 | 8.031 | 11.824 | 4.722 | 108.929 | 20.584 | |
| <i>ControlMM</i> -Medium-(8, 128, 250M) | | 0.617 | 0.757 | 0.819 | 6.335 | 36.355 | 14.502 | 20.908 | 7.869 | 11.250 | 4.676 | 102.677 | 18.132 | |
| <i>ControlMM</i> -Large-(16, 128, 478M) | | 0.604 | 0.744 | 0.809 | 7.872 | 36.169 | 15.964 | 23.476 | 8.169 | 11.625 | 4.752 | 113.027 | 19.368 | |

Table 5: **Ablation Study.** The results suggest that jointly modeling dynamic and static human skeleton topologies significantly improves performance. We found that freezing the body-wise en(de)coder helps retain the motion topology knowledge. We also validated the scalability of *ControlMM*. We design four scaling modeling variants, where $**-(a, b, c)$ denotes model $**$ with a transformer layer, b body-part encoding dimension, and total c parameter counts. Indicate best results.

| Method | $FID_H \downarrow$ | $FID_B \downarrow$ | Div \uparrow |
|-------------------------|--------------------|--------------------|----------------|
| Edge | 93.430 | 108.507 | 13.471 |
| Finedance | 10.747 | 72.229 | 13.813 |
| MCM | 4.717 | 78.577 | 14.890 |
| <i>ControlMM</i> -Basic | 3.858 | 76.248 | 16.667 |
| <i>ControlMM</i> -Mix | 4.825 | 124.935 | 20.742 |

Table 6: **Results of music-to-dance in FineDance of *ControlMM*-Bench.** We evaluate the FID_H , FID_B , and the diversity of *ControlMM* and SOTA baselines.

Indicate best results, Indicates second best results.

SOTA baselines, as shown in Tab. 6. Both variants of our model perform well in terms of diversity, attributed to the first stage of coarse text-to-motion generation training, which equips the model with extensive knowledge of motion topologies across various scenarios. However, it can be observed that *ControlMM*-Mix shows an increase in FID compared to *ControlMM*-Basic. This is likely due to the FineDance dataset's lack of necessary text descriptions, leading to identical pseudo-captions for different segments of the same song during the first stage of training. This one-to-many generation mode confuses when the model incorporates corresponding music information for each segment in the second stage, attempting to learn many-to-many relationships. Qualitative results in Fig. 4 show that *ControlMM* can generate natural dances according to the music beats.

Ablation Study

We conducted ablation experiments to verify the necessity of *ControlMM*-Attn design, the second stage training strategy, and scaling up influences. Results are in Tab. 5.

The necessity to decouple the static and dynamic human topology graph learning. We designed three *ControlMM*-Mix variants to investigate the impact of capturing human static and dynamic topological graphs: capturing no human topology, capturing only static topology, and capturing only dynamic topology. We have three key observations. **1 Modeling only static topology decreases performance in the text-to-motion task but significantly improves performance in speech-to-gesture and music-to-dance.** We attribute this to the static topology ensuring the model grasps basic spatial relations between body parts, enhancing gen-

eralization across various human motion scenarios. However, the additional learnable spatial structure module, unrelated to input, increases learning difficulty in the single text-to-motion task. **2 Only modeling dynamic topology nearly brings no benefits, not matching the large number of learnable parameters introduced.** This is because the initial optimization of the input-adaptive dynamic topology adjacency matrix is complex, especially for transferring topology knowledge against motion distribution drifts, making it hard for the model to converge to the correct dynamic topology. **3 Joint modeling of static and dynamic topologies effectively capture motion topology knowledge against distribution drifts**, as observed in human-centric research (Zeng et al. 2021). The static topology learns basic human structure, providing foundational spatial knowledge across tasks, while the dynamic topology adjusts according to specific motion distributions and control signals.

Freezing the body en(de)coder helps preserve the topology knowledge learned in stage-1. In the second stage of training, we found that whether to freeze the body encoder and body decoder also affects model performance. This is because they are responsible for encoding human motion into latent space and vice versa, partially influencing the modeling of human topological structure. We observed opposite performance trends in the second stage for speech-to-gesture and music-to-dance tasks when freezing and unfreezing these components. A possible explanation is that BEATS2 primarily involves lower body stillness and upper body gestures and facial movements, while FineDance and HumanML3D usually include whole-body movement. Therefore, unfreezing the body encoder and decoder in the second stage helps the model adjust to the topology in speech-to-gesture, while freezing them better preserves the topological priors learned for music-to-dance.

Scaling up impacts. Based on the acknowledgment of the scalability of transformer models, we explored the impact of model size on task performance. We increased the size of *ControlMM*-Mix from 77M to 478M, observing a rise-then-fall performance trend across three types of tasks as the model size increased with limited data. This verifies that increasing the model's parameter size can enhance generative capabilities, but without a corresponding increase in high-quality data, model performance may decline.

Conclusion

In this paper, we propose *ControlMM*, a unified framework for whole-body human motion generation with plug-and-play multimodal control that generalizes across different generative distributions and efficiently handles control signals of varying granularity. Our core design is *ControlMM-Attn*, which effectively learns and transfers motion knowledge across different distributions by parallel modeling of static and dynamic human topology graphs. *ControlMM* employs a coarse-to-fine training strategy that achieves fine-grained, plug-and-play control for control signals of varying low-level granularity without the optimization burden of mixed training. For a comprehensive evaluation, we introduce *ControlMM-Bench*, the first publicly available multimodal whole-body human motion generation benchmark based on the unified whole-body SMPL-X representation. Extensive experiments show that *ControlMM* achieves competitive performance across various motion generation tasks compared to state-of-the-art baselines.

References

Bian, Y.; Ju, X.; Li, J.; Xu, Z.; Cheng, D.; and Xu, Q. 2024. Multi-Patch Prediction: Adapting Language Models for Time Series Representation Learning. In *Forty-first International Conference on Machine Learning*.

Carreira, J.; Noland, E.; Hillier, C.; and Zisserman, A. 2019. A short note on the kinetics-700 human action dataset. *arXiv preprint arXiv:1907.06987*.

Chen, J.; Liu, Y.; Wang, J.; Zeng, A.; Li, Y.; and Chen, Q. 2024. DiffSHEG: A Diffusion-Based Approach for Real-Time Speech-driven Holistic 3D Expression and Gesture Generation. In *CVPR*.

Chen, X.; Jiang, B.; Liu, W.; Huang, Z.; Fu, B.; Chen, T.; and Yu, G. 2023. Executing your Commands via Motion Diffusion in Latent Space. In *Proceedings of the IEEE/CVF Conference on Computer Vision and Pattern Recognition*, 18000–18010.

Chung, J.; Wuu, C.-h.; Yang, H.-r.; Tai, Y.-W.; and Tang, C.-K. 2021. Haa500: Human-centric atomic action dataset with curated videos. In *Proceedings of the IEEE/CVF international conference on computer vision*, 13465–13474.

Gärtner, E.; Andriluka, M.; Coumans, E.; and Sminchisescu, C. 2022. Differentiable dynamics for articulated 3d human motion reconstruction. In *Proceedings of the IEEE/CVF conference on computer vision and pattern recognition*, 13190–13200.

Ginosar, S.; Bar, A.; Kohavi, G.; Chan, C.; Owens, A.; and Malik, J. 2019. Learning individual styles of conversational gesture. In *Proceedings of the IEEE/CVF Conference on Computer Vision and Pattern Recognition*, 3497–3506.

Girdhar, R.; El-Nouby, A.; Liu, Z.; Singh, M.; Alwala, K. V.; Joulin, A.; and Misra, I. 2023. Imagebind: One embedding space to bind them all. In *Proceedings of the IEEE/CVF Conference on Computer Vision and Pattern Recognition*, 15180–15190.

Gu, C.; Sun, C.; Ross, D. A.; Vondrick, C.; Pantofaru, C.; Li, Y.; Vijayanarasimhan, S.; Toderici, G.; Ricco, S.; Sukthankar, R.; et al. 2018. Ava: A video dataset of spatio-temporally localized atomic visual actions. In *Proceedings of the IEEE conference on computer vision and pattern recognition*, 6047–6056.

Guo, C.; Zou, S.; Zuo, X.; Wang, S.; Ji, W.; Li, X.; and Cheng, L. 2022. Generating Diverse and Natural 3D Human Motions From Text. In *Proceedings of the IEEE/CVF Conference on Computer Vision and Pattern Recognition (CVPR)*, 5152–5161.

Guo, C.; Zuo, X.; Wang, S.; Zou, S.; Sun, Q.; Deng, A.; Gong, M.; and Cheng, L. 2020. Action2motion: Conditioned generation of 3d human motions. In *Proceedings of the 28th ACM International Conference on Multimedia*, 2021–2029.

Hu, L. 2024. Animate anyone: Consistent and controllable image-to-video synthesis for character animation. In *Proceedings of the IEEE/CVF Conference on Computer Vision and Pattern Recognition*, 8153–8163.

Ionescu, C.; Papava, D.; Olaru, V.; and Sminchisescu, C. 2013. Human3. 6m: Large scale datasets and predictive methods for 3d human sensing in natural environments. *IEEE transactions on pattern analysis and machine intelligence*, 36(7): 1325–1339.

Kim, J.; Kim, J.; and Choi, S. 2023. Flame: Free-form language-based motion synthesis & editing. In *Proceedings of the AAAI Conference on Artificial Intelligence*.

Li, B.; Zhao, Y.; Zhelun, S.; and Sheng, L. 2022. Danceformer: Music conditioned 3d dance generation with parametric motion transformer. In *Proceedings of the AAAI Conference on Artificial Intelligence*.

Li, R.; Yang, S.; Ross, D. A.; and Kanazawa, A. 2021. Learn to Dance with AIST++: Music Conditioned 3D Dance Generation. *arXiv:2101.08779*.

Li, R.; Zhao, J.; Zhang, Y.; Su, M.; Ren, Z.; Zhang, H.; Tang, Y.; and Li, X. 2023. FineDance: A Fine-grained Choreography Dataset for 3D Full Body Dance Generation. In *Proceedings of the IEEE/CVF International Conference on Computer Vision*, 10234–10243.

Liang, H.; Bao, J.; Zhang, R.; Ren, S.; Xu, Y.; Yang, S.; Chen, X.; Yu, J.; and Xu, L. 2024. Omg: Towards open-vocabulary motion generation via mixture of controllers. In *Proceedings of the IEEE/CVF Conference on Computer Vision and Pattern Recognition*, 482–493.

Lin, J.; Zeng, A.; Lu, S.; Cai, Y.; Zhang, R.; Wang, H.; and Zhang, L. 2023. Motion-X: A Large-scale 3D Expressive Whole-body Human Motion Dataset. *Advances in Neural Information Processing Systems*.

Ling, Z.; Han, B.; Wong, Y.; Kangkanhalli, M.; and Geng, W. 2023. Mcm: Multi-condition motion synthesis framework for multi-scenario. *arXiv preprint arXiv:2309.03031*.

Liu, H.; Zhu, Z.; Becherini, G.; Peng, Y.; Su, M.; Zhou, Y.; Zhe, X.; Iwamoto, N.; Zheng, B.; and Black, M. J. 2024a. EMAGE: Towards Unified Holistic Co-Speech Gesture Generation via Expressive Masked Audio Gesture Mod-

eling. In *Proceedings of the IEEE/CVF Conference on Computer Vision and Pattern Recognition*, 1144–1154.

Liu, H.; Zhu, Z.; Iwamoto, N.; Peng, Y.; Li, Z.; Zhou, Y.; Bozkurt, E.; and Zheng, B. 2022a. Beat: A large-scale semantic and emotional multi-modal dataset for conversational gestures synthesis. In *European conference on computer vision*, 612–630. Springer.

Liu, J.; Dai, W.; Wang, C.; Cheng, Y.; Tang, Y.; and Tong, X. 2023. Plan, posture and go: Towards open-world text-to-motion generation. *arXiv preprint arXiv:2312.14828*.

Liu, J.; Shahroudy, A.; Perez, M.; Wang, G.; Duan, L.-Y.; and Kot, A. C. 2019. Ntu rgb+ d 120: A large-scale benchmark for 3d human activity understanding. *IEEE transactions on pattern analysis and machine intelligence*, 42(10): 2684–2701.

Liu, X.; Wu, Q.; Zhou, H.; Xu, Y.; Qian, R.; Lin, X.; Zhou, X.; Wu, W.; Dai, B.; and Zhou, B. 2022b. Learning hierarchical cross-modal association for co-speech gesture generation. In *Proceedings of the IEEE/CVF Conference on Computer Vision and Pattern Recognition*, 10462–10472.

Liu, Y.; Zhang, K.; Li, Y.; Yan, Z.; Gao, C.; Chen, R.; Yuan, Z.; Huang, Y.; Sun, H.; Gao, J.; He, L.; and Sun, L. 2024b. Sora: A Review on Background, Technology, Limitations, and Opportunities of Large Vision Models. *arXiv:2402.17177*.

Loper, M.; Mahmood, N.; Romero, J.; Pons-Moll, G.; and Black, M. J. 2015. SMPL: A Skinned Multi-Person Linear Model. *ACM Trans. Graphics (Proc. SIGGRAPH Asia)*, 34(6): 248:1–248:16.

Lu, S.; Chen, L.-H.; Zeng, A.; Lin, J.; Zhang, R.; Zhang, L.; and Shum, H.-Y. 2023. HumanTOMATO: Text-aligned Whole-body Motion Generation. *arxiv:2310.12978*.

Luo, M.; Hou, R.; Chang, H.; Liu, Z.; Wang, Y.; and Shan, S. 2024. M3-GPT: An Advanced Multimodal, Multi-task Framework for Motion Comprehension and Generation. *arXiv preprint arXiv:2405.16273*.

Mahmood, N.; Ghorbani, N.; Troje, N. F.; Pons-Moll, G.; and Black, M. J. 2019. AMASS: Archive of motion capture as surface shapes. In *Proceedings of the IEEE/CVF international conference on computer vision*, 5442–5451.

Nie, Y.; Nguyen, N. H.; Sinthong, P.; and Kalagnanam, J. 2022. A time series is worth 64 words: Long-term forecasting with transformers. *arXiv preprint arXiv:2211.14730*.

Pavlakos, G.; Choutas, V.; Ghorbani, N.; Bolkart, T.; Osman, A. A. A.; Tzionas, D.; and Black, M. J. 2019. Expressive Body Capture: 3D Hands, Face, and Body from a Single Image. In *Proceedings IEEE Conf. on Computer Vision and Pattern Recognition (CVPR)*, 10975–10985.

Punnakkal, A. R.; Chandrasekaran, A.; Athanasiou, N.; Quiros-Ramirez, A.; and Black, M. J. 2021. BABEL: Bodies, action and behavior with english labels. In *Proceedings of the IEEE/CVF Conference on Computer Vision and Pattern Recognition*, 722–731.

Rombach, R.; Blattmann, A.; Lorenz, D.; Esser, P.; and Ommer, B. 2022. High-resolution image synthesis with latent diffusion models. In *Proceedings of the IEEE/CVF conference on computer vision and pattern recognition*, 10684–10695.

Shazeer, N.; Mirhoseini, A.; Maziarz, K.; Davis, A.; Le, Q.; Hinton, G.; and Dean, J. 2017. Outrageously large neural networks: The sparsely-gated mixture-of-experts layer. *arXiv preprint arXiv:1701.06538*.

Siyao, L.; Yu, W.; Gu, T.; Lin, C.; Wang, Q.; Qian, C.; Loy, C. C.; and Liu, Z. 2022. Bailando: 3d dance generation by actor-critic gpt with choreographic memory. In *Proceedings of the IEEE/CVF Conference on Computer Vision and Pattern Recognition*, 11050–11059.

Taheri, O.; Ghorbani, N.; Black, M. J.; and Tzionas, D. 2020. GRAB: A dataset of whole-body human grasping of objects. In *Computer Vision–ECCV 2020: 16th European Conference, Glasgow, UK, August 23–28, 2020, Proceedings, Part IV 16*, 581–600. Springer.

Tang, Y.; Liu, J.; Liu, A.; Yang, B.; Dai, W.; Rao, Y.; Lu, J.; Zhou, J.; and Li, X. 2023. FLAG3D: A 3D Fitness Activity Dataset with Language Instruction. In *CVPR*.

Team, G.; Anil, R.; Borgeaud, S.; Wu, Y.; Alayrac, J.-B.; Yu, J.; Soricut, R.; Schalkwyk, J.; Dai, A. M.; Hauth, A.; et al. 2023. Gemini: a family of highly capable multimodal models. *arXiv preprint arXiv:2312.11805*.

Tevet, G.; Raab, S.; Gordon, B.; Shafir, Y.; Cohen-or, D.; and Bermano, A. H. 2023. Human Motion Diffusion Model. In *The Eleventh International Conference on Learning Representations*.

Trivedi, N.; Thatipelli, A.; and Sarvadevabhatla, R. K. 2021. NTU-X: an enhanced large-scale dataset for improving pose-based recognition of subtle human actions. In *Proceedings of the Twelfth Indian Conference on Computer Vision, Graphics and Image Processing*, 1–9.

Tseng, J.; Castellon, R.; and Liu, K. 2023. Edge: Editable dance generation from music. In *Proceedings of the IEEE/CVF Conference on Computer Vision and Pattern Recognition*, 448–458.

Vaswani, A.; Shazeer, N.; Parmar, N.; Uszkoreit, J.; Jones, L.; Gomez, A. N.; Kaiser, Ł.; and Polosukhin, I. 2017. Attention is all you need. *Advances in neural information processing systems*, 30.

Yi, H.; Liang, H.; Liu, Y.; Cao, Q.; Wen, Y.; Bolkart, T.; Tao, D.; and Black, M. J. 2023. Generating Holistic 3D Human Motion from Speech. In *CVPR*.

Zeng, A.; Sun, X.; Yang, L.; Zhao, N.; Liu, M.; and Xu, Q. 2021. Learning skeletal graph neural networks for hard 3d pose estimation. In *Proceedings of the IEEE/CVF international conference on computer vision*, 11436–11445.

Zhang, J.; Yan, H.; Xu, Z.; Feng, J.; and Liew, J. H. 2023a. MagicAvatar: Multi-modal Avatar Generation and Animation. In *arXiv:2308.14748*.

Zhang, J.; Zhang, Y.; Cun, X.; Huang, S.; Zhang, Y.; Zhao, H.; Lu, H.; and Shen, X. 2023b. T2M-GPT: Generating Human Motion from Textual Descriptions with Discrete Representations. In *Proceedings of the IEEE/CVF Conference on Computer Vision and Pattern Recognition (CVPR)*.

Zhang, L.; Rao, A.; and Agrawala, M. 2023. Adding conditional control to text-to-image diffusion models. In *Proceedings of the IEEE/CVF International Conference on Computer Vision*, 3836–3847.

Zhang, M.; Cai, Z.; Pan, L.; Hong, F.; Guo, X.; Yang, L.; and Liu, Z. 2024a. Motondiffuse: Text-driven human motion generation with diffusion model. *IEEE Transactions on Pattern Analysis and Machine Intelligence*.

Zhang, M.; Jin, D.; Gu, C.; Hong, F.; Cai, Z.; Huang, J.; Zhang, C.; Guo, X.; Yang, L.; He, Y.; et al. 2024b. Large motion model for unified multi-modal motion generation. *arXiv preprint arXiv:2404.01284*.

Zhang, M.; Li, H.; Cai, Z.; Ren, J.; Yang, L.; and Liu, Z. 2023c. FineMoGen: Fine-Grained Spatio-Temporal Motion Generation and Editing. *NeurIPS*.

Zhang, S.; Ma, Q.; Zhang, Y.; Qian, Z.; Kwon, T.; Pollefeys, M.; Bogo, F.; and Tang, S. 2022. Egobody: Human body shape and motion of interacting people from head-mounted devices. In *European conference on computer vision*, 180–200. Springer.

Zhou, Z.; Wan, Y.; and Wang, B. 2023. A unified framework for multimodal, multi-part human motion synthesis. *arXiv preprint arXiv:2311.16471*.

Zhuang, W.; Wang, C.; Chai, J.; Wang, Y.; Shao, M.; and Xia, S. 2022. Music2dance: Dancenet for music-driven dance generation. *ACM Transactions on Multimedia Computing, Communications, and Applications (TOMM)*, 18(2): 1–21.